

Numerical simulations of the XR-5 Hall thruster for life assessment at different operating conditions

Alejandro Lopez Ortega^{*}, Benjamin A. Jorns^{*}, Ioannis G. Mikellides[†] and Richard R. Hofer[‡]
Jet Propulsion Laboratory, California Institute of Technology, Pasadena, CA, 91109

Abstract: NASA’s Jet Propulsion Laboratory has been investigating the applicability of Aerojet Rocketdyne’s XR-5 thruster, a 4.5 kW class Hall thruster, for deep-space missions. Major considerations for qualifying the XR-5 for deep-space missions are demonstration of a wide throttling envelope and a usable life capability in excess of 10,000 h. Numerical simulations with the 2-D axisymmetric code Hall2De are employed to inform the qualification process by assessing erosion rates at the thruster surfaces in a wide range of throttling conditions without the need for conducting costly endurance testing. In previous work at JPL by Jorns et al., the anomalous collision frequency distribution for 11 different throttling conditions of the XR-5 spanning 0.3-4.5 kW were identified based on probe measurements of the electron temperature in the near plume region. In this paper, we provide estimates for the erosion rates at the channel walls and pole covers for the same 11 conditions. Uncertainties in the plasma measurements and in the anomalous collision frequency distribution are addressed by determining upper and lower bounds of the erosion rates. Results suggest that erosion of the walls only occurs in the last 5% of the acceleration channel and the rate of such erosion decreases as the geometry of the thruster changes in time due to magnetic shielding. A quasi-zero-erosion state is eventually achieved in all the examined throttling conditions. Examination of the results for pole surface erosion and estimated cathode life indicates that the XR-5 propellant throughput capability will exceed 700 kg, which provides 50% margin over the usable throughput capability of 466 kg as already demonstrated in wear testing

Nomenclature

| | | |
|---------------------|---|--|
| β | = | incidence angle of ions on thruster walls |
| Δt | = | time-step in Hall2De numerical simulation |
| $d_{emitter}$ | = | cathode emitter thickness (in μm) |
| ε | = | erosion rate |
| ε_{max} | = | maximum erosion rate |
| f_{β} | = | contribution of incidence angle to sputtering yield |
| f_K | = | contribution of ion kinetic energy to sputtering yield |
| iF | = | index used to denote a particular ion population |
| iz | = | index used to denote a particular ion charge state |
| I_d | = | discharge current |
| I_{keeper} | = | cathode keeper current |
| j_i | = | ion current density |
| K | = | ion kinetic energy |
| K_{plasma} | = | ion kinetic energy due to acceleration in computational domain |

^{*} Member of the Technical Staff, Electric Propulsion Group, 4800 Oak Grove Drive, Pasadena, CA, 91109, Mail Stop 125-109, Member AIAA.

[†] Principal Engineer, Electric Propulsion Group, 4800 Oak Grove Drive, Pasadena, CA, 91109, Mail Stop 125-109, AIAA Associate Fellow.

[‡] Senior Engineer, Electric Propulsion Group, 4800 Oak Grove Drive, Pasadena, CA, 91109, Mail Stop 125-109, AIAA Associate Fellow.

Copyright 2015 California Institute of Technology. U.S. Government sponsorship acknowledged.

| | | |
|-------------------|---|--|
| K_{sheath} | = | ion kinetic energy due to acceleration in infinitesimal sheath |
| K_T | = | threshold ion energy for sputtering to occur |
| L | = | acceleration channel length |
| MFR | = | neutral mass flow rate |
| N_F | = | number of ion populations |
| N_z | = | number of ion charge states |
| ν_{ei} | = | electron-ion collision frequency |
| ν_{en} | = | electron-neutral collision frequency |
| ν_{anom} | = | anomalous collision frequency |
| r | = | radial coordinate |
| $R_{midchannel}$ | = | radial location of acceleration channel centerline |
| $t_{emitter}$ | = | emitter expected life (in h) |
| $T_{emitter}$ | = | emitter temperature (in K) |
| V_d | = | discharge voltage |
| $\omega_{e,Gyro}$ | = | electron cyclotron frequency |
| Y | = | sputtering yield |
| z | = | axial coordinate |

I. Introduction

Several missions identified in the most recent NASA Planetary Decadal Survey are enabled by the use of solar electric propulsion (SEP) systems. In order to provide a wide range of SEP options to the mission planning community proposing electric propulsion for competed missions, NASA has been partnering with several commercial suppliers with the aim of qualifying for deep space applications existing electric propulsion thruster technology currently used for Earth-orbit station keeping and orbit transfer. Due to the higher flight rate of commercial thrusters, production and qualification costs are estimated to be reduced by as much as 50% with respect to government-built systems [1].

The Aerojet Rocketdyne XR-5 is a commercial, 4.5 kW-class, Hall effect thruster with excellent potential for application to deep space missions attending to its wide throttling envelope [1-3] and the quasi-zero-erosion state that was achieved after approximately 5,000 hours of operation at high power conditions [4-5] due to magnetic shielding. The XR-5 has also demonstrated flight performance, having been flown successfully on three of the Air Force's Advanced EHF satellites, where it is employed for partial orbit transfers and station-keeping in geosynchronous Earth orbit [6]. These characteristics suggest the potential utilization of the XR-5 in missions requiring in excess of 10,000 hours of operation. However, life qualification through endurance testing reflective of a realistic mission profile is impractical due to scheduling limitations of vacuum facilities and to the uncertainty of the exact throttling profiles required. The need for practical life qualification may be replaced by numerical simulations validated by plasma measurements over a discrete set of operating conditions that span the throttling envelope of the thruster. The results of these computations can in turn be employed to produce estimates of erosion rates at the thruster surfaces. The principal limitation of these simulations lies in the uncertainty associated with the source of anomalous transport of electrons across magnetic field lines known to persist [7] in Hall effect thrusters. After many decades of research considerable progress has been made on identifying the source(s) of the anomalous transport in Hall thrusters [8-12] and on incorporating such physics in codes like Hall2De [13]. However, to this point a first-principles model of anomalous resistivity in Hall thruster plasma codes with sufficient fidelity remains elusive [13-17]. Therefore until such self-consistent models have been completed, simulations need to be informed by experimental measurements to accurately capture the principal features of the plasma (i.e., the steep plasma potential gradient that determines the acceleration region and the location of the peak in electron temperature) with respect to the thruster geometry and magnetic field topology [18]. However, once such measurements are in place (as in the case of the present work), physics-based codes like Hall2De become powerful tools in the thruster life qualification process. Adding to the complexity of this endeavor, it is now known that the injection of plasma probes upstream of the peak magnetic field location in Hall thrusters perturbs the plasma and, in consequence, the measurements [19]. These perturbations appear to become larger as power density increases.

The JPL in-house numerical code for the simulation of the plasma discharge in Hall thrusters, Hall2De [20-21], includes an implementation of the anomalous transport of electrons by means of an effective anomalous collision frequency that acts in lowering the Hall parameter [18]. Anomalous collision frequency profiles that produce

numerical solutions consistent with experimental measurements in other thrusters, such as the H6 [19,21-22], have been previously identified and the lessons learned from those investigations on the variation of the anomalous collision frequency in the computational domain have been applied in simulations of the XR-5. In a previous paper [23], candidate anomalous collision frequency profiles were identified for eleven throttling conditions of the XR-5 ranging from 0.3 kW to 4.5 kW with discharge voltages in the range of 150 to 400 V. Due to the multiple choices available in the selection of a possible anomalous collision frequency profile and the limited number of experimental measurements at each operating condition, three guidelines were followed: the computed discharge current must agree with the experimental value, the predicted thrust must be within 15% of the measured thrust, and the electron temperature downstream of its peak along the acceleration channel centerline must be in close agreement with the experimental measurements inferred from injected emissive probes. Plasma solutions and performance variables based on these profiles were also reported.

In this paper, we evaluate, by means of numerical simulations, the estimated throughput of the XR-5 thruster. Three potential life-limiting mechanisms are examined: erosion of the channel walls, erosion of the pole surfaces, and cathode life. A description of the XR-5 thruster and the eleven throttling conditions used in this study are given in Section II. In Section III, a brief description of the numerical code, Hall2De, is given and the sputtering yield models used for the different thruster surfaces presented. In Section IV, erosion rates with the anomalous collision frequency profiles found in [23] are computed. At this point, we find that uncertainties in the plasma location due to probe perturbation can have an important effect on our erosion predictions. These uncertainties are quantified in Section V, completed with a new set of simulations that provide an upper and lower bound to the erosion predictions. We complete our assessment of operating life of the XR-5 giving estimates of emitter life and wall erosion for the cathode in Section VI.

II. Description of the XR-5 thruster and throttling conditions

The XR-5 is a 4.5-kW Hall thruster developed in a joint effort between Lockheed Martin Space Systems and Aerojet Rocketdyne. Its main purpose at the time of conception was to be used in geostationary satellite applications for station keeping and orbit raising operations [4,24-26]. Several thrusters of this type have been flown to date on the Advanced EHF spacecraft [6].

The Qualification Life Test (QLT) for GEO applications [4] revealed that the thruster reaches a nearly zero-erosion state for the channel walls after approximately 5,600 hours of operation. High-power conditions ranging from 3 kW to 4.5 kW were employed during this test. Numerical simulations by JPL using Hall2De were used to identify the physics responsible for the thruster reaching a near zero-erosion state [5], which was referred to as magnetic shielding. Magnetic shielding aims at producing a zero-erosion state in Hall thrusters by defining a magnetic field topology with lines that graze the thruster walls and extend deep in the channel towards the anodes, forcing low electron temperatures along such grazing lines.

Following the QLT, several Qualification Extension Tests (QET) were performed. The first was NASA funded and focused on extended operation at low power (1-2 kW). The qualification thruster has also been operated down to 0.3 kW by Aerojet Rocketdyne [26] and extensive low-power testing has been performed by JPL with the Engineering Model 2 (EM2) thruster down to as low as 0.15 kW [27].

More recently, Aerojet Rocketdyne restarted the Qualification Life Test (QLT) of the XR-5 under JPL funding and in partnership with Lockheed Martin [28]. The thruster had last been operated in July 2008 and at that point had reached 10,400 h of operation [4]. Qualification Extension Test 4 (QET4) was successfully started and demonstrated thruster operation spanning 0.6-4.5 kW. Operation at 0.6 kW exceeded the 1.0 kW minimum power demonstrated in previous qualification testing, with performance consistent with other measurements on the EM2 XR-5 at JPL [27]. QET4 was interrupted due to a ground test facility issue that prohibited further testing of the thruster. The precise cause of the issue and potential mitigation is under investigation by Aerojet Rocketdyne. As summarized in Table I, QET4 accumulated 342 h of operation and processed 14.1 kg of xenon propellant, bringing the total demonstrated propellant throughput of the XR-5 to 466 kg of xenon as shown in Table I. The demonstrated throttling range and throughput capability makes this thruster a promising candidate to be used in cost-capped mission categories such as the Discovery or New Frontiers programs.

| Parameter | QET4 | Total |
|----------------------------|------|--------|
| Firing time (h) | 342 | 10,740 |
| Thruster Starts | 35 | 7,351 |
| Cathode Starts | 38 | 7,386 |
| Impulse (MN-s) | 0.27 | 8.98 |
| Propellant throughput (kg) | 14.1 | 466 |

Table I: Demonstrated capability of the XR-5 Hall thruster from QET4 and total values.

The first set of numerical simulations considered in this paper assume a thruster with channel rings that replicate the geometry found after 6,800[§] hours of operation in the QLT. A similar geometry that mimics the channel geometry after 9,600[§] hours of test was previously employed for assessments of thruster performance and investigations related to the magnetic shielding principles [5]. The latter configuration is employed here in Section V in order to verify that the erosion rates (found to be significant in the last section of the channel walls for the 6,800-h configuration in Section IV) effectively decrease with time of operation as the thruster walls are eroded. The channel walls in the configuration being simulated in this paper are made of boron nitride, while an alumina coating is employed at the inner and outer pole surfaces. Sputtering yield models for these materials are given in the next section.

The operating conditions that are considered in the numerical simulations are summarized in Table II. The conditions that were primarily tested in the QLT were the high power – high voltage pairs used for GEO applications: 300V-3kW, 300V-4.5kW, 400V-7.5kW, and 400V-11.25kW. Erosion predictions for all the listed cases are given in Section IV.

| Discharge voltage, V_d (V) | Discharge current, I_d (A) | Power (kW) |
|------------------------------|------------------------------|------------|
| 150 | 2 | 0.3 |
| 200 | 2 | 0.4 |
| 200 | 5 | 1.0 |
| 300 | 2 | 0.6 |
| 300 | 3.33 | 1.0 |
| 300 | 5 | 1.5 |
| 300 | 10 | 3.0 |
| 300 | 15 | 4.5 |
| 400 | 5 | 2.0 |
| 400 | 7.5 | 3.0 |
| 400 | 11.25 | 4.5 |

Table II: XR-5 throttling conditions considered in Hall2De numerical simulations.

III. Computational method

A. General description of Hall2De

Hall2De is a numerical code for the simulation of the plasma discharge in Hall effect thrusters that has been developed at the Jet Propulsion Laboratory over the last decade. Its most notable features are described here whilst the interested reader can find the specifics of the numerical implementation in [20-21]. In Hall2De, a quadrilateral-based computational grid aligned with the magnetic field is employed. A typical simulation domain comprises the acceleration channel and a region of the plume that extends several times the length of the channel in the radial and axial directions. Cylindrical geometry is assumed, with the axis being the thruster centerline, in a way such that equations of motion are only solved in the axial and radial directions. This simplification is particularly beneficial in the case of cathodes mounted at the thruster centerline but requires certain approximations to be made when

[§]The terms 6,800 and 9,600 hours do not correspond exactly (but rather approximately) to the operating time at which the geometry was measured. However, this notation has been used in previous publications and we follow it here for the aim of consistency.

configurations with cathodes mounted off-center, such as the XR-5, are employed. In this case, the cathode boundary condition is replicated by an annular surface whose inner and outer radius is given by the location of the keeper orifice of the hollow cathode. The electron current emanating from the cathode is distributed uniformly in the azimuthal direction in order to preserve the cylindrical symmetry in the computational domain.

The motion of each of the species in the plasma is solved separately. The density and velocity distribution of neutral particles is modeled using free-molecular flow, according to the view-factor algorithm described in [29]. Ions are modeled using a hydrodynamic approach in which they are divided into multiple populations (or “fluids”), iF , attending to their energy. Typically two populations are sufficient: ions with high and low energy, generated upstream (beam ions) and downstream (plume ions) of the acceleration region, respectively. Separate continuity and momentum equations are solved for each population and each charge state, iz , which can take values from 1 (singly charged ions) to 3 (triple charged ions). Ions of different fluids and charge states can interact with one another through ionization, charge exchange, and elastic collisions. The distinction between populations of high and low energy ions was introduced in the numerical code after establishing that collisions in the plume region are typically scarce enough such that beam and plume ions are not necessarily in equilibrium with one another [21]. Attempting to solve all the motion of ions as a single population would result in reduced values of plasma density in the plume, as can be inferred from a continuity argument where the large velocity of the beam ions dominates over the low speeds of ions generated downstream of the acceleration region. The effect of using multiple ion populations over a single population was quantified in [21]. Since under-predicting the concentration of ions in the pole regions can result in reduced erosion rates, all the simulations featured in this article use the two-population approach. The threshold between the two is established by the maximum kinetic energy that an ion generated at a particular location would achieve, which can be approximated by the local plasma potential.

Electron motion is modeled using a fluid approach where inertia is neglected. This approach results in a vector form of Ohm’s law that is solved in the directions parallel and perpendicular to the magnetic field lines and enables computation of the plasma potential when combined with current conservation and the assumption of plasma quasi-neutrality. Electron temperature is determined as the solution of an energy conservation equation [20]. The non-classical (collision-less) transport of electrons in the thruster plume and acceleration channel is included in the model through the use of an effective anomalous collision frequency defined along the channel centerline and extrapolated following magnetic field lines [18]. The shape of this profile has been modified as new experimental measurements have become available until reaching a general qualitative shape that can be applied to any thruster with no major modifications. It is shown in [22] that even though the specifics of the plasma properties inside the acceleration channel cannot be determined by the use of injected probes [19], changes in the anomalous collision profile inside the channel with the aim of bounding experimental uncertainties have little effect on the plasma solution in the plume.

B. Sputtering yield models

Two different materials are considered in the sputtering yield models for the XR-5 thruster. The walls of the acceleration channel are made of boron nitride (BN), while an alumina (Al_2O_3) coating is used at the inner and outer poles. Erosion in Hall2De accounts for contributions from three charge states, Xe^+ , Xe^{++} and Xe^{+++} , for each ion population. The sputtering erosion rate, ε , due to ion bombardment by ions of charge state iz and population iF is given by,

$$\varepsilon_{iz,iF} = j_{iz,iF} Y_{iz,iF} \quad , \quad (1)$$

where the component of the incident ion current density perpendicular to the channel wall, $j_{iz,iF}$, can be computed from the ion number density ($n_{iz,iF}$) and the ion velocity ($u_{iz,iF}$) at the wall. The sputtering yield, Y , is a function of the ion impact energy $K_{iz,iF}$, and incidence angle of the ions, β , which is computed as the arctangent of the ratio between the tangential and perpendicular (with respect to the wall) velocity components of the ions. Y is expressed here in units of mm^3/C unless otherwise noted. The total erosion rate is the sum over all populations and all charge states:

$$\varepsilon = \frac{\sum_j \sum_{i=1}^{N_i} \sum_{iF=1}^{N_{iF}} \varepsilon_{iz,iF} \Delta t_j}{\sum_j \Delta t_j} \quad . \quad (2)$$

Because ions must traverse a sheath before striking the wall, the total impact energy is the sum of the kinetic energy ions have acquired in the plasma upon entrance to the sheath, and the sheath potential energy. The latter, transformed to ion kinetic energy as the plasma ions are accelerated inside the sheath towards the solid material, is computed based on the Hobbs and Wesson solution to the 1-D sheath equations in the presence of secondary electron emission [30]. The total impact energy is then $K=K_{plasma}+ K_{sheath}$, and the incidence angle, β can be computed based on the ion velocities perpendicular and parallel to the walls. A factorization of the sputtering yield is assumed:

$$Y = f_{\beta}(\beta)f_k(K), \quad (3)$$

where $f_{\beta}(\beta)$ and $f_k(K)$ are fitting functions for the angular and energy dependence (at zero angle of incidence), respectively.

The angular dependence of xenon on boron nitride is implemented using a fit of Garnier et al.'s [31] to Yamamura's function [32] for the angular yield:

$$f_{\beta}(\beta) = \cos(\beta)^{-c_0} \exp\left[-c_1(\cos(\beta)^{-c_2} - 1)\right] \quad (4)$$

The coefficients c_0 , c_1 , and c_2 take the values 2.5204, 0.8552 and 1.0, respectively. Since no data for the angular dependence for alumina is available, the same fit is employed in the alumina simulations. As seen in Fig. 1 (right), the angular yield can increase the erosion rates by approximately a factor of 3 at high incidence angles (up to 80 degrees). It is shown in Section IV that erosion of the pole surfaces is mostly produced by beam ions, which have large incidence angles since their motion is mostly tangential to the walls. Thus, pole erosion results can be over-estimated if the angular yield for alumina is not as large as for boron nitride at large angles (erosion rates will be over-estimated by at most a factor of 3) or if the decay of the angular yield to zero as the incidence angle increases begins for lower angles (over-estimation by one or two orders of magnitude may occur as the decay to zero angular yield is very steep). On the other hand, under-estimation of the pole erosion rates by more than an order of magnitude is extremely unlikely to occur as the peak value of angular yield for alumina would need to be significantly higher than for boron nitride.

The energy contribution to the sputtering yield for boron nitride follows the expression proposed by Bohdanský [33] with fit to the data in [34]:

$$f_{K,BN}(K) = A \left(1 - \frac{K_T}{K}\right)^2 \left(1 - \left(\frac{K_T}{K}\right)^{2/3}\right), \quad (5)$$

with $A = 0.035$ and $K_T = 35$ eV. K_T represents the energy threshold below which there is no erosion of the material surfaces. As seen in Fig. 1, the exact value for K_T is uncertain due to lack of experimental measurements at low energies. We estimate that the threshold energy is in the range from 25 to 50 eV and have chosen the value of 35 eV for these simulations since this value produces the closest agreement to the measured erosion rates at the channel walls in the H6 thruster [21]. The expression for the sputtering yield in alumina was derived from Eckstein's model [35-36] and has the expression:

$$f_{K,Al_2O_3}(K) = Aq s_n(\bar{\varepsilon}) \frac{\left(\frac{K}{K_T} - 1\right)^{\mu}}{\lambda + \left(\frac{K}{K_T} - 1\right)^{\mu}}, \quad (6)$$

with $\bar{\varepsilon} = K / K_L$ and s_n is computed as:

$$s_n(\bar{\varepsilon}) = \frac{0.5 \ln(1 + 1.2288\bar{\varepsilon})}{\bar{\varepsilon} + 0.1728\sqrt{\bar{\varepsilon}} + 0.008\bar{\varepsilon}^{0.1504}}. \quad (7)$$

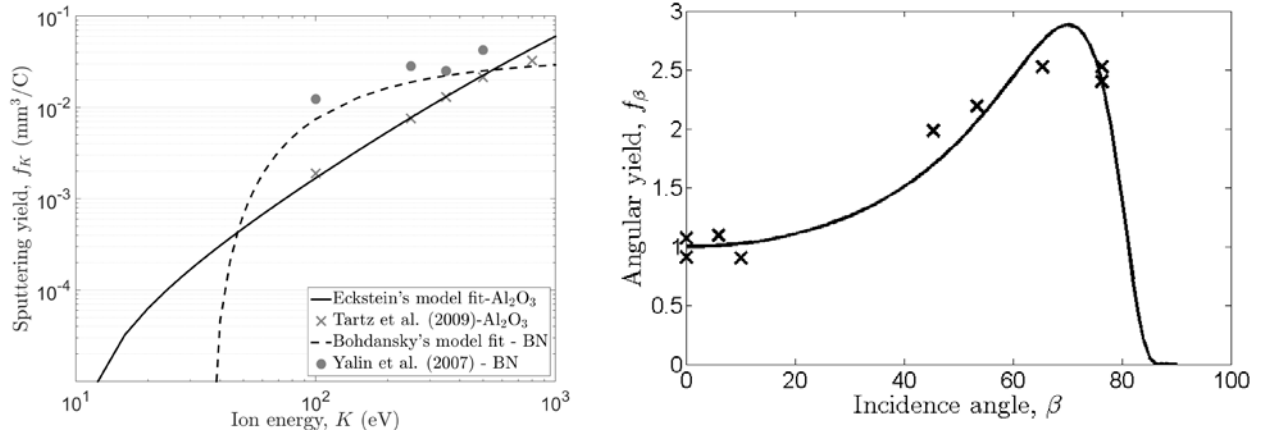


Fig. 1. Left: Sputtering yield for perpendicular xenon ion bombardment on boron nitride (BN) and alumina (Al_2O_3). Comparison between implemented fit (5-7) and experimental data. Right: Angular yield model using Yamamura's function [32] and comparison with experimental measurements by Garnier et al. [31].

The values for the coefficients in the expressions above that produce a good fit with the experimental data by Tartz et al. [37] are: the conversion from atoms/ion to mm^3/C , $A = 0.035$, $q = 25$ atoms/ion, $\lambda = 400$, $\mu = 1$, $K_L = 6.94 \times 10^5$ eV (a quantity related to the Lindhard screening length [35]), and $K_T = 10$ eV. A comparison between the experimental data and the numerical models for boron nitride and alumina is shown in Fig. 1, where the model for the contribution of the incident angle to the sputtering yield is also depicted.

IV. Numerical results and erosion rates

The electron temperature and plasma potential along the channel centerline for the 400V-4.5kW operating condition are shown in Fig. 2. Experimental measurements are also depicted for comparison. The electron temperature profile shows good agreement with the measurements in the plume, where experimental results should not be excessively perturbed by the presence of the probes. The peak electron temperature however is larger by

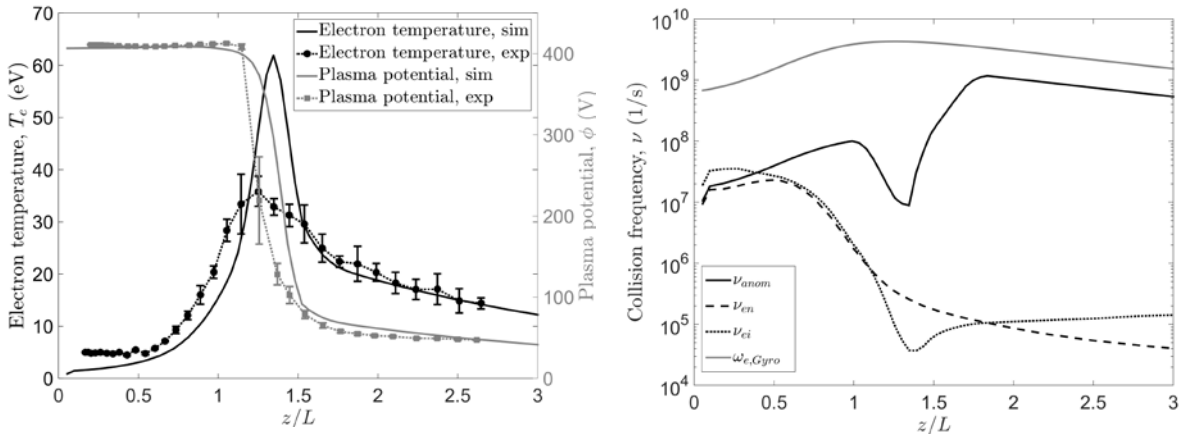


Fig. 2. Left: Plasma potential and electron temperature in the 400V-4.5kW operating condition and comparison with experimental measurements by emissive probes along the channel centerline. Note that in order to obtain good agreement with the electron temperature in the plume region, the difference in peak electron temperatures between numerical simulations and experiments becomes very large. Right: Anomalous collision frequency profile employed in the 400V-4.5kW case and comparison with classical collision frequencies and electron cyclotron frequency.

approximately

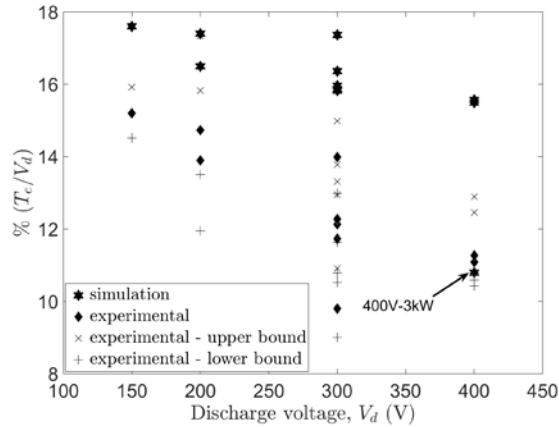


Fig. 3. Ratio of peak electron temperature with respect to discharge voltage (in %) for different throttling conditions. Numerical simulations indicate that the ratio is approximately constant except for the “anomalous” 400V-3kW case. Numerical simulation results exhibit a negative slope in the ratio of electron temperature with respect to discharge voltage as the voltage increases. Agreement between simulations and experiments is better at low power conditions, in which the plasma is less perturbed by the injection of probes. Upper and lower bounds for the experimental measurements are also provided.

a factor of two in the numerical simulations. In the acceleration region, large probe perturbations are to be expected and experimental results are, by consequence, uncertain. The comparison between the numerical and experimental plasma potential profiles also exhibits good agreement in the plume. The anomalous collision frequency profile employed in this simulation is shown in Fig. 2 (right). The typical features of this profile, common to other thrusters, are the large value (close to the cyclotron frequency and much larger than the classical collision frequencies) of the anomalous collision frequency in the plume, where the Hall parameter is close to unity, and the dip that establishes the position of the acceleration region. The shape of the profile upstream of the dip has been the subject of recent investigations, motivated by the fact that probe-based plasma measurements inside the channel are uncertain. The results of tests run with different profiles upstream of the acceleration region appear to indicate that closer agreement with global performance variables in the thruster is achieved when the profile becomes flat (instead of increasing, as in this case) upstream of the acceleration region [22]. The plasma properties described for the 400V-4.5kW case are qualitatively followed by the other throttling conditions, except for the 400V-3kW case. The latter is a consequence of the uncertainties in the exact location of the acceleration region and will be discussed further in Section V. As an example, in Fig. 3, the peak electron temperature for each throttling condition is plotted scaled with the discharge voltage. We compare this with the trend noted in [38-39], where it is stated that the peak electron temperature stays roughly proportional (by a factor of approximately 0.12) to the discharge voltage for a wide variety of examined thrusters. It can be observed that the over-estimation of the peak electron temperature with respect to the experimental results occurs in all cases, except for the 400V-3kW case. At the same time, numerical and experimental results are in closer agreement at low power conditions (over-estimation occurs by a factor of approximately 1.2 at low power conditions and 1.8 at high power conditions). This latter phenomenon can be a consequence of the plasma being less perturbed by the probe injection at lower power settings, as indicated in [19].

Ion energy, ion current, and erosion rates at the different thruster walls for the 400V-4.5kW case are shown in Fig. 4. At the channel walls, no erosion is observed except for a region very close to the channel exit (i.e., $z/L > 0.95$). However, the erosion rates in this region are significant, with a maximum value of 4×10^{-1} mm/kh at the inner channel (which would produce an erosion of four millimeters after 10,000 hours of operation if the rate is constant). The erosion produced close to the exit region of the channel is produced by the acceleration of ions starting slightly upstream of the channel exit, as observed by the increase in ion energy at $z/L > 0.9$ and the decrease in ion current density. Due to the localized effect of the erosion, the likely result in extended operation conditions would be a more rounded channel exit. Results with the more eroded configuration, which represents the geometry after 9,600 hours of the QLT (relative to the 6,800 hours in the current configuration) are shown in Section V.

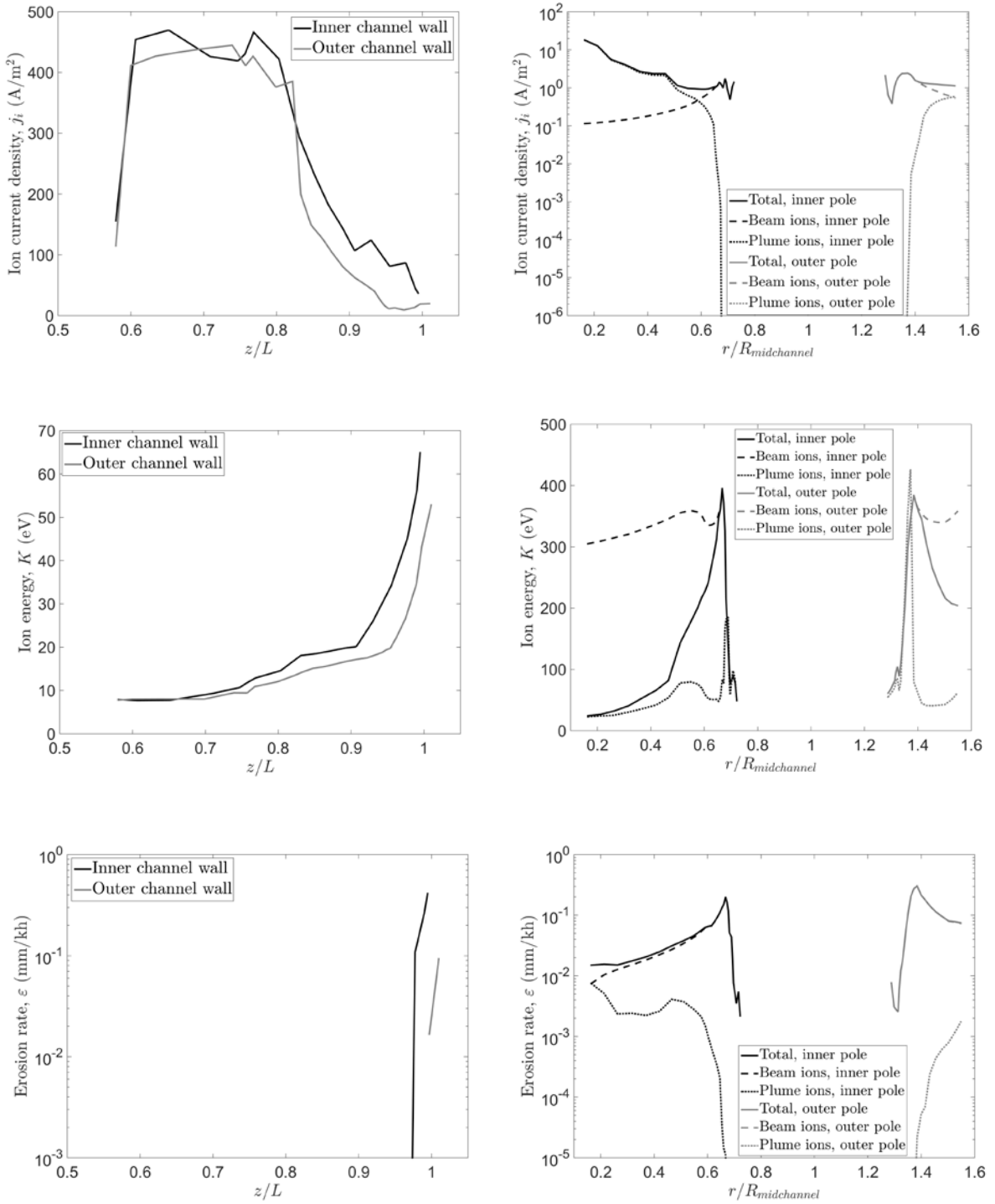


Fig. 4. Average ion energy, ion current and erosion rates at the thruster walls for the 400V-4.5kW operating condition. Left: values for the inner and outer channel as a function of the axial location. Right: values for the inner and outer poles as a function of the radial location. Along the poles, the contribution of high-energy beam ions and low-energy plume ions is depicted.

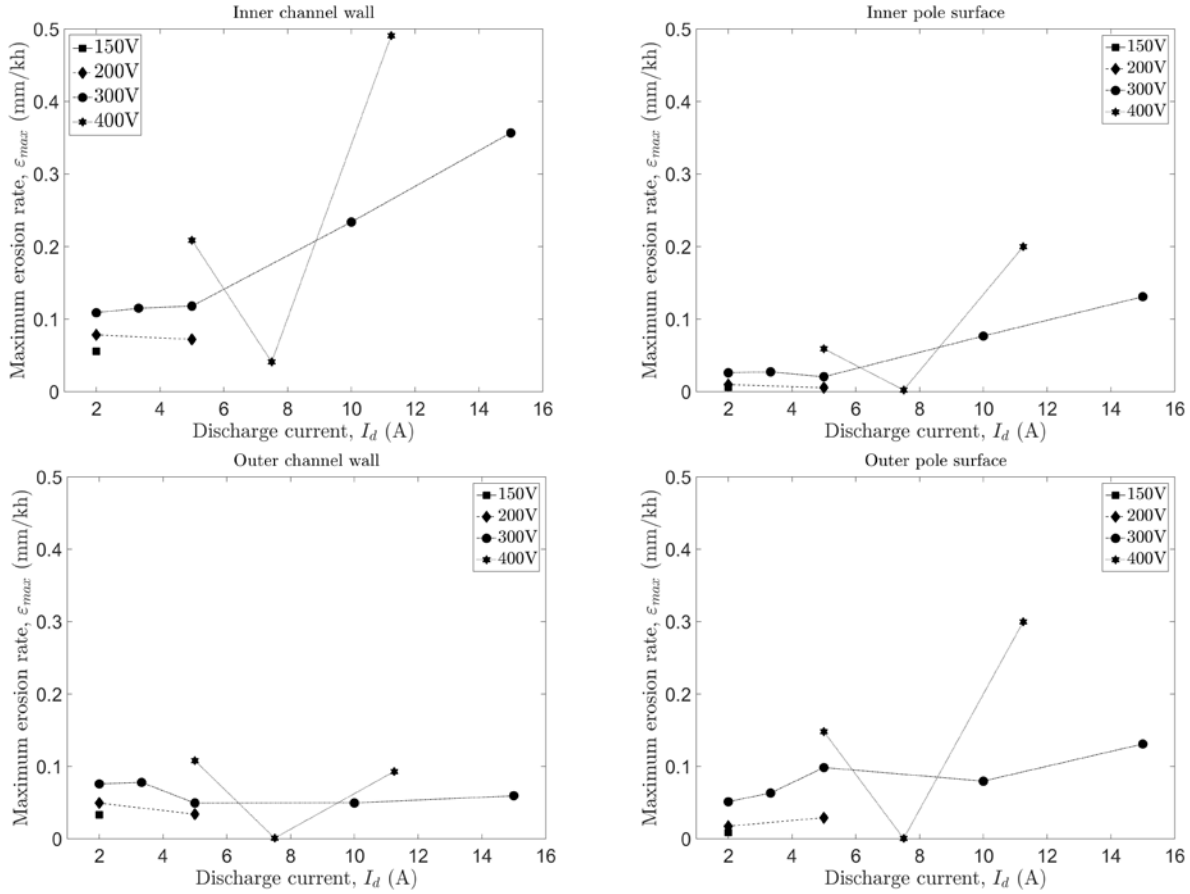


Fig. 5. Maximum erosion rates along the channel and pole walls as a function of the operating condition. Note that the results for the 400V-7.5A-3kW case are not consistent with the trends established by the rest of the data points, which indicate an increase in the erosion rate with voltage and current.

With respect to pole erosion, we depict, in addition to the total erosion rate, the separate contributions of plume and beam ions. Beam ions contribute the most to the erosion of the poles, a consequence of the high divergence of the beam in the XR-5. The erosion is more acute close to the channel due to the increased current of high-energy ions and their large energy, close to 400 V on average. Ions produced in the near plume do not contribute significantly to the erosion owing to their low energy (in the range of 50 to 100 V). Current density of low-energy ions is only significant far from the channel. It is important to note that the peaks observed in the ion energy of plume ions in the vicinity of the channel are numerical artifacts produced by the diffusion built in the discretization of the equations of motion, which leads to a minimal fraction of plume ions that move against the potential gradient. This phenomenon has no effect on the erosion rates due to the negligible ion currents associated with the numerical diffusion process. The observed peak erosion rates are similar to those found in the channel walls, with maximum values in the vicinity of 2×10^{-1} mm/kh.

The features described for the 400V-4.5kW case (channel erosion only occurring in the close vicinity of the channel exit and erosion of the poles due to the high divergence of the ion beam) are qualitatively similar to those found in all the other operating conditions (with the exception of the 400V-3kW case). In Fig. 5, the peak erosion rates at the channel walls and pole covers are plotted for all the considered throttling conditions. Neglecting the atypical 400V-3kW case for the moment, results clearly indicate that there exists an increase in erosion rates with discharge voltage (due to the higher energy of the ions) and with current (due to associated higher mass flow rate that in turn results in larger values of the ion current density). In consequence, the limiting case in terms of erosion is the 400V-4.5kW condition. The increase in erosion rate with discharge current appears to be more abrupt at large current conditions and at the inner surfaces (pole coating and channel) than at the outer surfaces. The 400V-3kW

case is clearly not typical when compared to the other throttling conditions, exhibiting peak erosion rates that are an order of magnitude (or more) lower in all the thruster surfaces.

The results shown in this section suggest that the uncertainties associated with both the simulation and measurement of the plasma properties along the channel centerline can have an effect on the predicted erosion rates. The peak electron temperature in simulations is always over-estimated, especially at high-power conditions in which the erosion rates are higher, but the values of the temperature in the plume are always in close agreement with the experiments. The only case (400V-3kW-7.5A) with a peak electron temperature similar to the experiments exhibits erosion rates in all the surfaces that are lower, in comparison to other high-power cases, by at least one order of magnitude. In addition, it is known that plasma measurements can be largely perturbed in the acceleration region, which may result in the agreement between simulations and experimental measurements for the peak temperature in the 400V-3kW case being merely coincidental. These questions are addressed in the next section.

V. Lower and upper bounds of the erosion rates

In this section, we investigate the features of the plasma simulations that led to the observed differences in the computed erosion rates between the 400V-3kW case and the rest of operating conditions. Using this information, we bound the erosion rates for the “best-case” and “worst-case” scenarios. The results shown in the previous section also revealed that erosion of the poles and of the channel wall corners close to the channel exit occurs in the 6,800-h geometry. In order to evaluate whether the predicted erosion rates decrease as erosion continues to change the shape of the channel rings beyond the 6,800-h configuration, we estimate the erosion rate at a more advanced erosion state, representative of the geometry encountered in the XR-5 after 9,600 hours of operation in the QLT.

A. Plasma properties in the 400V-3kW operating condition. “High temperature” and “low temperature” profiles

Figure 6 provides a clear picture of the main differences between the plasma properties in the 400V-3kW and 400V-4.5kW cases. We have chosen the latter for comparison since it is the operating condition with higher erosion rates and both operating conditions are at the same discharge voltage. The contour plots for the plasma potential indicate that in the 400V-3kW case, the acceleration region is moved upstream by a short distance. The plasma potential in the plume is also higher in the lower power case. In consequence, the electron temperature decreases substantially as it is mostly determined in this region by the effect of Ohmic heating. The plasma density contours help explain the lower erosion rates in the 400V-3kW condition. As the acceleration region is moved upstream, the beam is less divergent and fewer ions are deflected to locations close to the poles. The ion density in the vicinity of the poles is approximately two orders of magnitude lower in the 400V-3kW operating condition. At the same time, as the plasma potential gradient accelerates the ions in the axial direction, charged particles are not allowed to “graze” the chamfered region of the acceleration channel. Even though the energy of the ions that bombard the channel walls may be larger (as they have been accelerated by the plasma potential gradient upstream), their density is too low to produce significant erosion. In the higher power setting, the acceleration region is located right at the channel exit. The ions, which have low velocity upstream of the acceleration region, graze the channel walls in the chamfered region and produce significant erosion as they are slightly accelerated at the very end of the channel. Since more ions are close to the channel walls, the number of them that are deflected towards the poles is also higher.

The results discussed above are associated with the details of the model profile used for the anomalous collision frequency. These profiles in [23] yield good agreement with the electron temperature in the plume (where measurements are not perturbed) and predict the thrust within 15% of the measured value. The electron temperature measurements have been used to guide the anomalous frequency model rather than the plasma potential as the experimental uncertainty in the first is smaller than that in the second. In Fig. 7, we show that two different anomalous collision frequency profiles can yield solutions that are acceptable within the uncertainties of our measurements. We called these profiles hereinafter “low temperature” and “high temperature” according to the peak value of the electron temperature they produce. The profile used in the previous section for the 400V-3kW case was the “low temperature” profile, which resulted in low erosion rates, the plasma properties shown in Fig. 6, and good

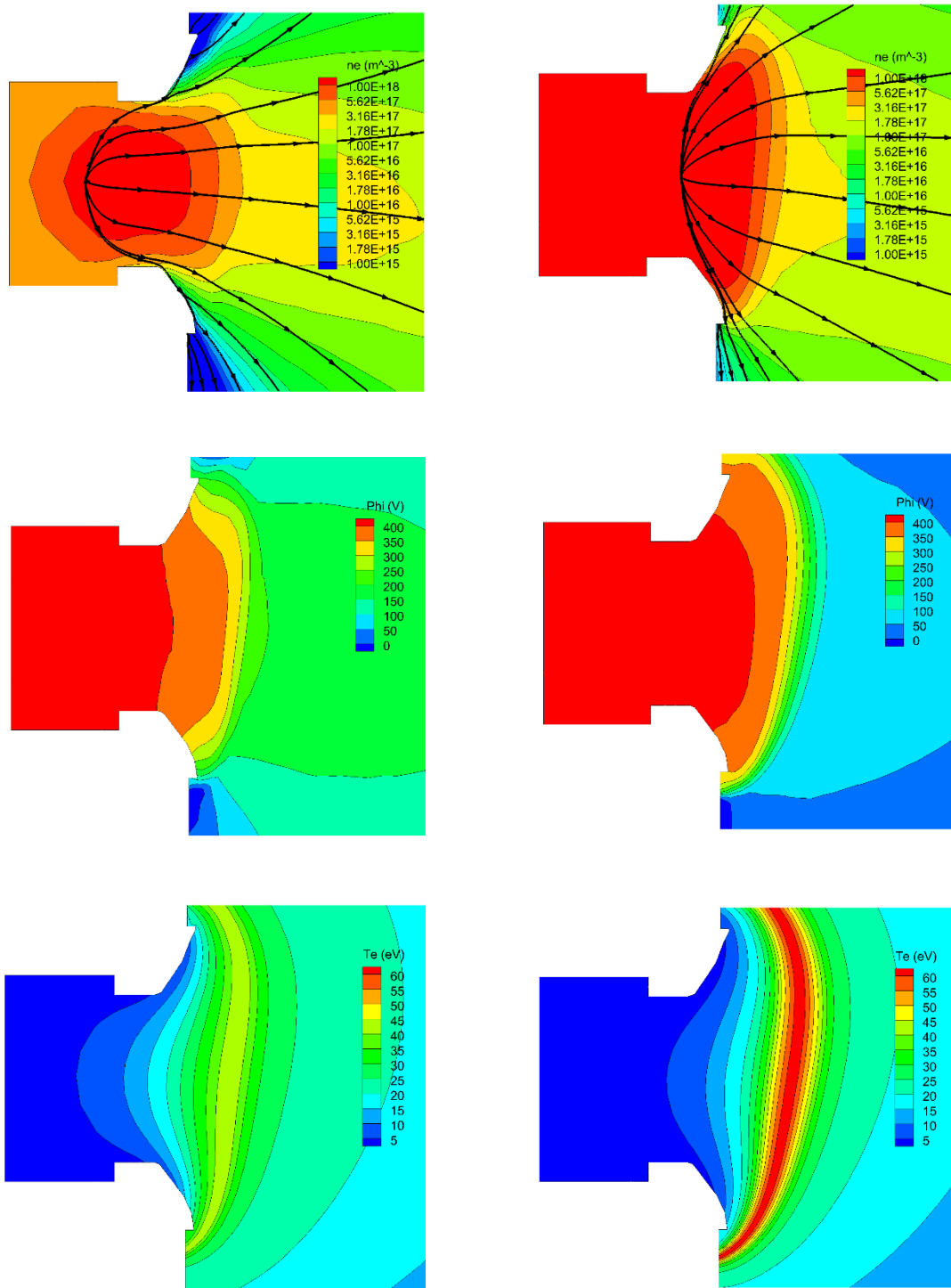


Fig. 6. Contour plots of plasma properties in the 400V-3kW (left) and 400V-4.5kW (right) cases. From top to bottom: plasma density and trajectories of beam ions, plasma potential, and electron temperature. It can be observed that the location of the acceleration region has been moved upstream in the 400V-3.0kW condition, resulting in lower electron temperatures and an ion beam with less divergence, which in turn reduces the erosion of the poles.

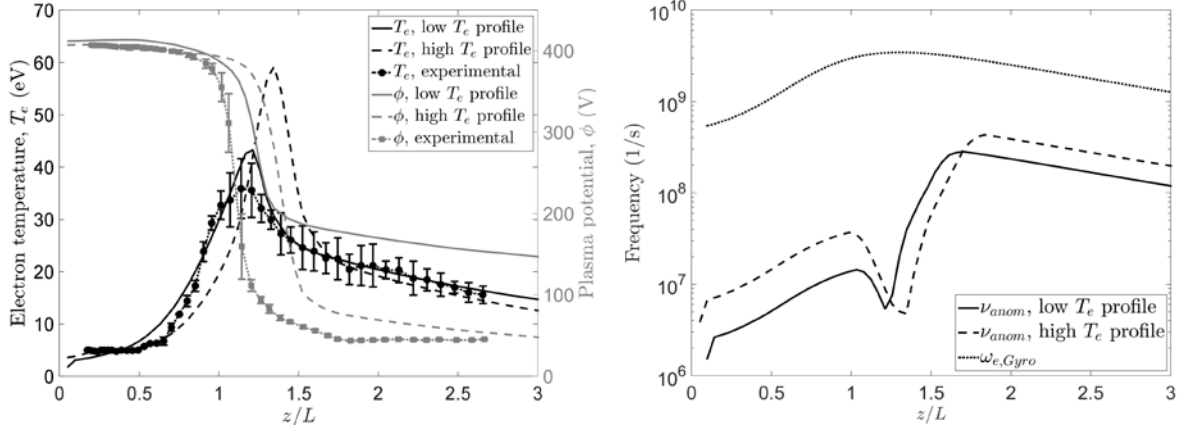


Fig. 7. Left: electron temperature, plasma potential, and comparison with experimental measurements for the low and high electron temperature profile used for the 400V-3kW operating condition. Right: anomalous collision frequency profiles used in the low and high peak electron temperature cases.

agreement with the measured peak electron temperature (even though the latter may be inaccurate due to plasma perturbations produced by the injected probes). However, this solution produces a plume plasma potential value in the range of 150 V, very far from the measured 40 V. Even though the plasma potential measurements were believed to be less accurate than the electron temperature measurements, a ~ 100 V uncertainty in the plume potential seems unlikely, especially when probe perturbations are known to be lower in the plume region. We can also produce a solution for the 400V-3kW case with an anomalous collision profile that is similar to the one used in the 400V-4.5kW case. This is a “high temperature profile” located more downstream and that produces a higher value of the peak electron temperature (in line with the other operating conditions examined) and a lower value of the potential in the plume. It is shown in Fig. 7 (right) that the “high temperature profile” (dashed line) and the “low temperature profile” (continuous line) are not very dissimilar and that both result in electron temperatures in the plume that exhibit good agreement with the experimental measurements. With respect to performance, the predicted thrust is 150 mN and 165 mN for the “low temperature” and “high temperature” profiles, respectively, both within 15% of the measured value of 175 mN. The original profile produces less thrust due to the higher plume potential, which leads to less net acceleration of the ions. This deficit is only partially compensated by the ion beam being more focused along the z -axis. In a similar fashion, as shown in Fig. 8, a “low temperature” anomalous collision

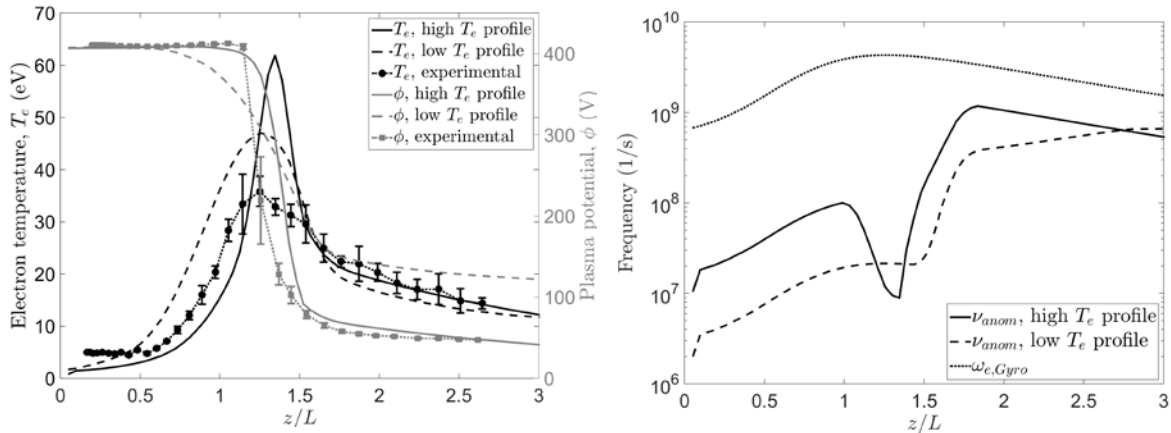


Fig. 8. Left: electron temperature, plasma potential, and comparison with experimental measurements for the low and high electron temperature profile used for the 400V-4.5kW operating condition. Right: anomalous collision frequency profiles used in the low and high peak electron temperature cases.

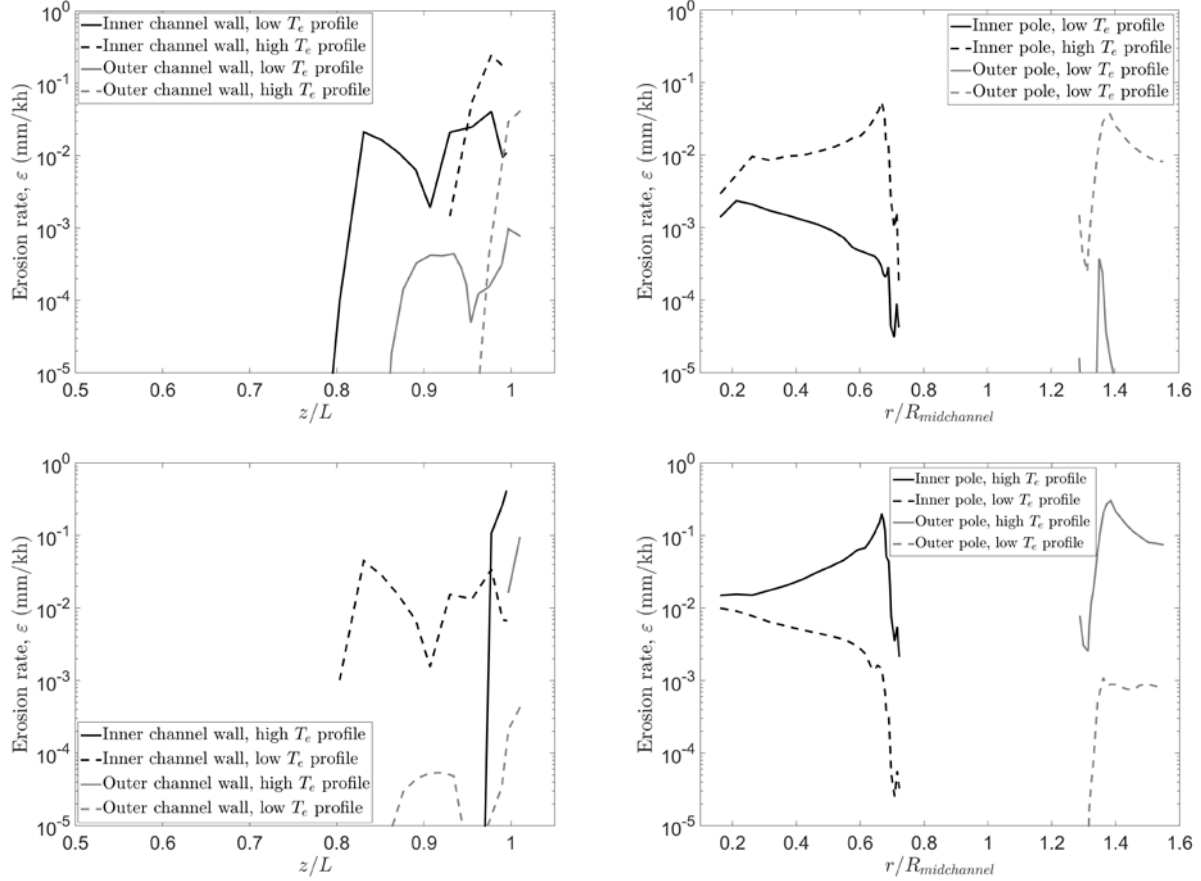
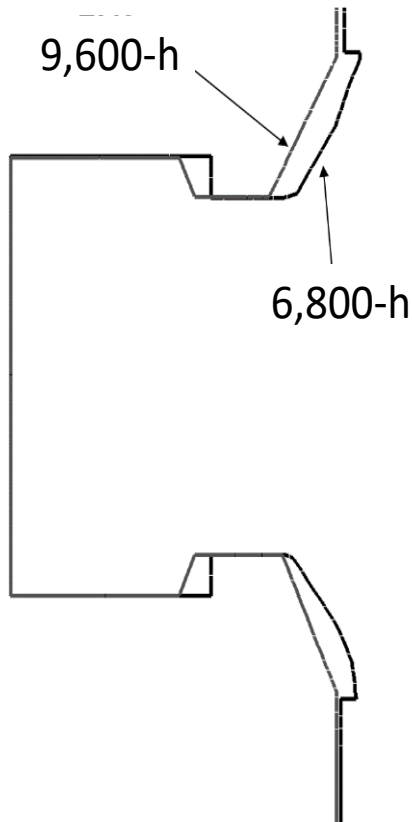


Fig. 9. Erosion rates at the thruster walls for the 400V-3kW (top) and 400V-4.5kW (bottom) conditions with high and low peak electron temperature profiles. In all cases, the maximum erosion rates decrease by at least one order of magnitude. However, erosion appears upstream in the acceleration channel in the low peak electron temperature cases due to changes in the location of the acceleration region.

frequency profile can be proposed for the 400V-4.5kW case (as the original profile used for the computations in Section IV was a “high temperature” profile). In this case we have adopted a flat anomalous collision frequency profile for the initial half of the channel, consistent with the shapes being currently used for other magnetically shielded thrusters, such as the H6MS [40]. The features in plasma potential and electron temperature along the channel centerline are similar to those encountered in the 400V-3kW case, with special relevance to the large plume potential (on the order of 150 V). With respect to thrust measurements, both profiles are within 15% of the experimental value (257 mN), with the “high temperature profile” yielding 232 mN and the “low temperature”, 219 mN. The “low temperature profile” was originally favored for the 400V-3kW case because plasma measurements indicated that the peak electron temperature was located slightly upstream of the 400V-2kW and 400-4.5kW cases (Fig. 6 in [23]) and also due to the good agreement with the measured electron temperature in the acceleration region (even when this measurement can have a large uncertainty associated with it). A “high temperature” profile predicts higher temperatures (by factors close to 2) than the measured values. It is important to note that all the attempts to produce an anomalous collision frequency profile that could combine low peak electron temperature and low values of the plasma potential in the plume failed. This is because the peak in the electron temperature is mainly driven by Ohmic heating in the acceleration region. In the “low temperature” profile, the total potential drop from the channel to the plume decreases and so does the total Ohmic heating, resulting in lower peak temperatures. The opposite effect occurs with a “high temperature” profile. The presence at the same time of lower peak electron temperatures and low plasma potential in the plume does not appear to be possible attending to the electron energy equation of Hall2De [20].

The erosion rates along each thruster surface for the profiles described above in the 400V-3kW and 400V-4.5kW cases are shown in Fig. 9. The “high temperature” profiles for both operating conditions yield qualitatively similar results, with erosion only occurring at the very end of the acceleration channel and at the pole covers. Using the “low temperature profile” in the 400V-4.5kW leads to lower maximum erosion rates in all surfaces by at least an order of magnitude. These rates are in line with the original results presented for the “low temperature profile” in the 400V-3kW condition. Even though the peak values for the erosion rates in the “low temperature profile” are lower, it is also shown in Fig. 9 that the erosion extends further upstream in the acceleration channel. This is a consequence of the acceleration region being also upstream, producing in turn high energy ions inside the channel. Since these ions do not tend to graze the channel walls, as observed in Fig. 6, the erosion of the channel walls would be very low, less than a millimeter after 10,000 hours of operation.

The results shown here indicate that the atypical data-point in Fig. 5 for the 400V-3kW case is a consequence of using an anomalous collision frequency profile that yields lower values of the electron temperature in the acceleration region. The use of a different anomalous collision frequency profile that yields a higher peak electron temperature but that still results in plasma properties and performance predictions in close agreement with the experimental measurements produces erosion rates that are consistent with the trends defined by simulations at other throttling conditions. At the same time, we can use the “high temperature” and “low temperature” types of anomalous collision frequency profiles to establish upper and lower bounds to the erosion rates. Due to time constraints and given that the “low temperature profile” results in lower erosion rates, only the 400V-4.5kW and the 400V-3kW cases were examined in detail, although a similar behavior is expected in other throttling conditions.



B. Erosion rates in the 9600-h geometry

Erosion rate predictions computed in Section IV indicate that the sputtering of the channel walls, albeit restricted to the surfaces in close proximity to the channel exit, could result in erosion depths of several millimeters after 10,000 hours of operation. Erosion rates of the poles were comparable. The Qualification Life Test indicates that a quasi-steady state in the geometry of the XR-5 was observed after approximately 5,060 hours of operation at high power settings (300 and 400V at 3 and 4.5 kW). However, a comparison between the 6,800-h and the 9,600-h geometries (Fig. 10) suggest that some erosion still occurs, especially at the chamfered region close to the channel exit. In order to assess the evolution of the observed erosion rates with operation time, we conducted numerical simulations using the more eroded geometry. A simulation was run at the most demanding power condition for each discharge voltage (150, 200, 300, and 400 V). The anomalous collision frequency profiles used in these computations was the same employed for the simulations in Section IV and are, in consequence, worst-case scenario, “high temperature” profiles.

Fig. 10. Channel geometry for the 6800-h and 9600-h configurations. The difference in geometry at the “throat” of the acceleration channel in the 9600-h geometry is a modeling simplification and does not affect the features of the acceleration region, which is located further downstream.

Figure 11 depicts the plasma density and electron temperature contours in the 6,800-h and 9,600-h geometries for the 400V-4.5kW case. Plasma density is not significantly perturbed by the change in geometry and the ion trajectories are approximately the same. With respect to the electron temperature, it can be observed that the magnetic shielding of the thruster is slightly better in the 9,600-h configuration, as lower electron temperatures are found close to the walls. A key aspect of the magnetic shielding principle [5] is the

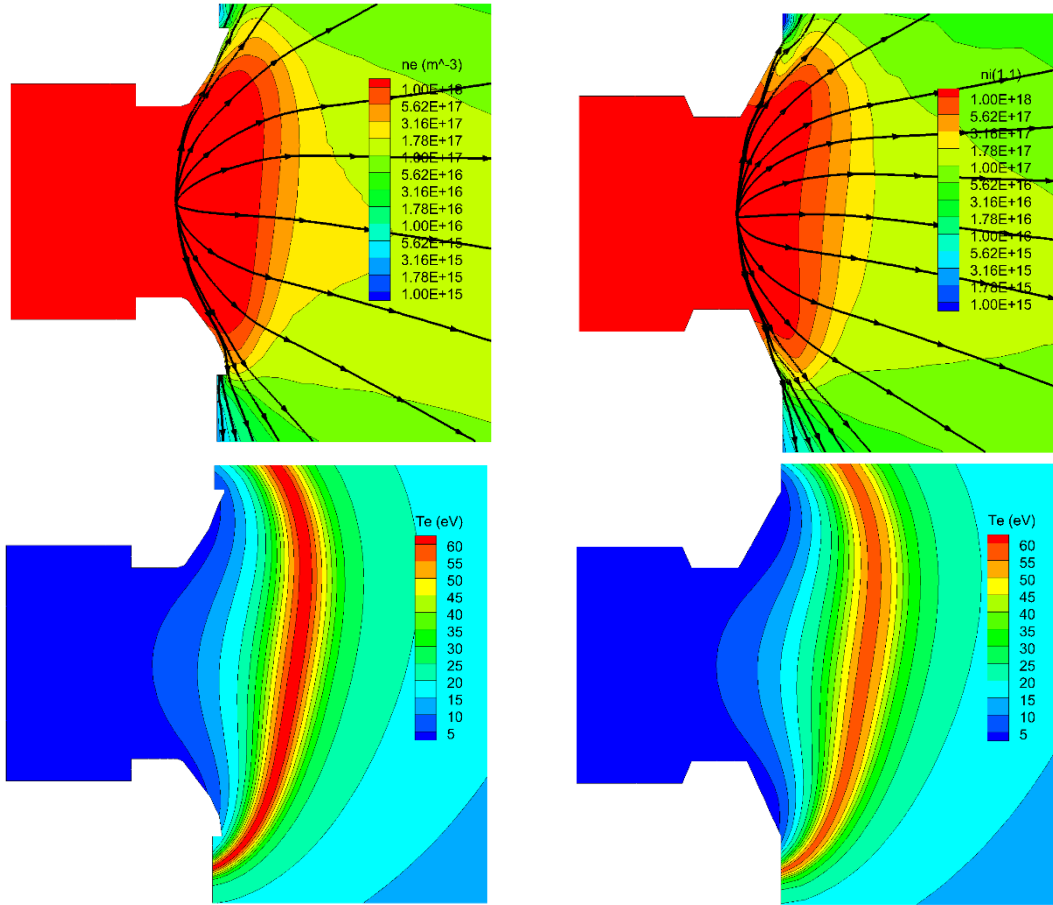


Fig. 11. Contour plots of plasma density (top) and electron temperature (bottom) for the 400V-4.5kW throttling condition (high peak electron temperature profile) in the 6,800-h and 9,600-h geometries. No significant changes in the plasma density occur between the two configurations. Due to progressive erosion of the chamfered channel walls, the thruster achieves a better shielding condition (lower electron temperature at the walls) in the 9,600-h configuration.

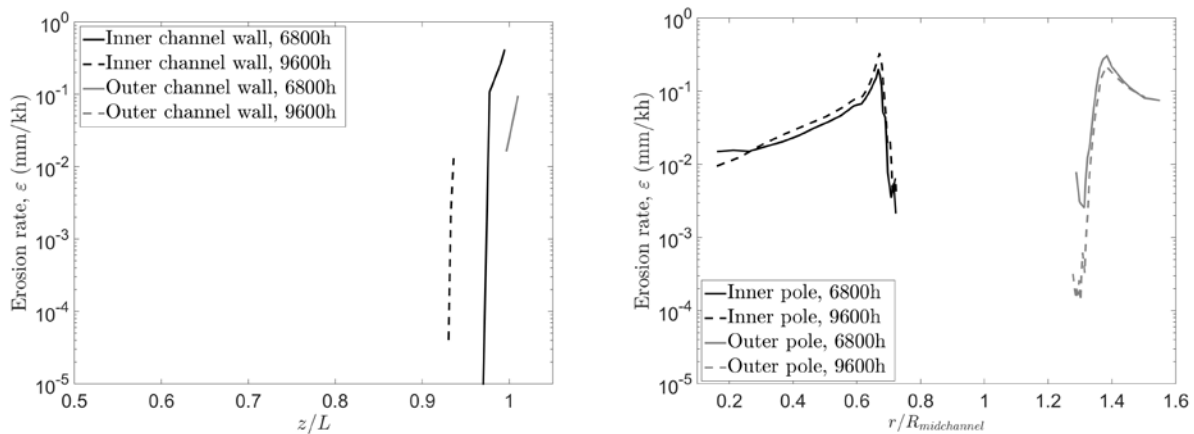


Fig. 12. Erosion rates at the thruster walls in the 6,800-h and 9,600-h channel configurations for the 400V-4.5kW condition with high peak electron temperature profile. In the 9,600-h geometry, erosion only persists extremely close to the channel exit and has decreased by an order of magnitude with respect to the 6,800-h configuration (note that L is still defined as the length of the channel in the 6,800-h configuration). Pole erosion is not largely affected by the change in geometry.

establishment of small variations in the plasma potential along magnetic field lines that graze the walls. In order to achieve this, Boltzmann's relation for electrons indicates that changes in the potential values due to variation of the plasma density along magnetic field lines are more acute as the electron temperature increases. By lowering the value of the electron temperature, changes in plasma density become progressively more irrelevant and quasi-equipotentialization of magnetic field lines is achieved. In the 9,600-h configuration, temperatures in excess of 5 eV are achieved only close to the tip of the inner ring, while in the 6,800-h configuration, electron temperatures of more than 10 eV are present in the same region. The same applies to the outer channel ring.

In Fig. 12, the erosion rates for the 400V-4.5kW throttling condition are shown in the 6,800-h and 9,600-h configurations. As predicted by our previous discussion on the electron temperature close to the channel walls and its effect on the magnetic shielding of the thruster, the erosion at the inner channel walls is reduced in the 9,600-h configuration by more than an order of magnitude. The effect in the outer channel is even more pronounced, with no erosion being predicted in the 9,600-h geometry. With respect to the erosion at the poles, the change in configuration has no significant effect, and predicted results are similar for both geometries. These results suggest that even when the erosion can be relatively large at the channel rings close to the exit, progressive erosion of the ring tip leads to a geometry with better magnetic shielding of the walls and smaller erosion rates. Results (in terms of maximum erosion rates) for the simulations run with the 9,600-h geometry for 150, 200, and 300 V are given in the next subsection, which summarizes the numerical investigation of the erosion rates at the thruster surfaces of the XR-5.

C. Summary of results for maximum erosion rates

The maximum erosion rates computed for each surface and operating condition are summarized in Fig. 13. We have augmented the results shown in Fig. 5 with the erosion rates computed in the numerical investigations

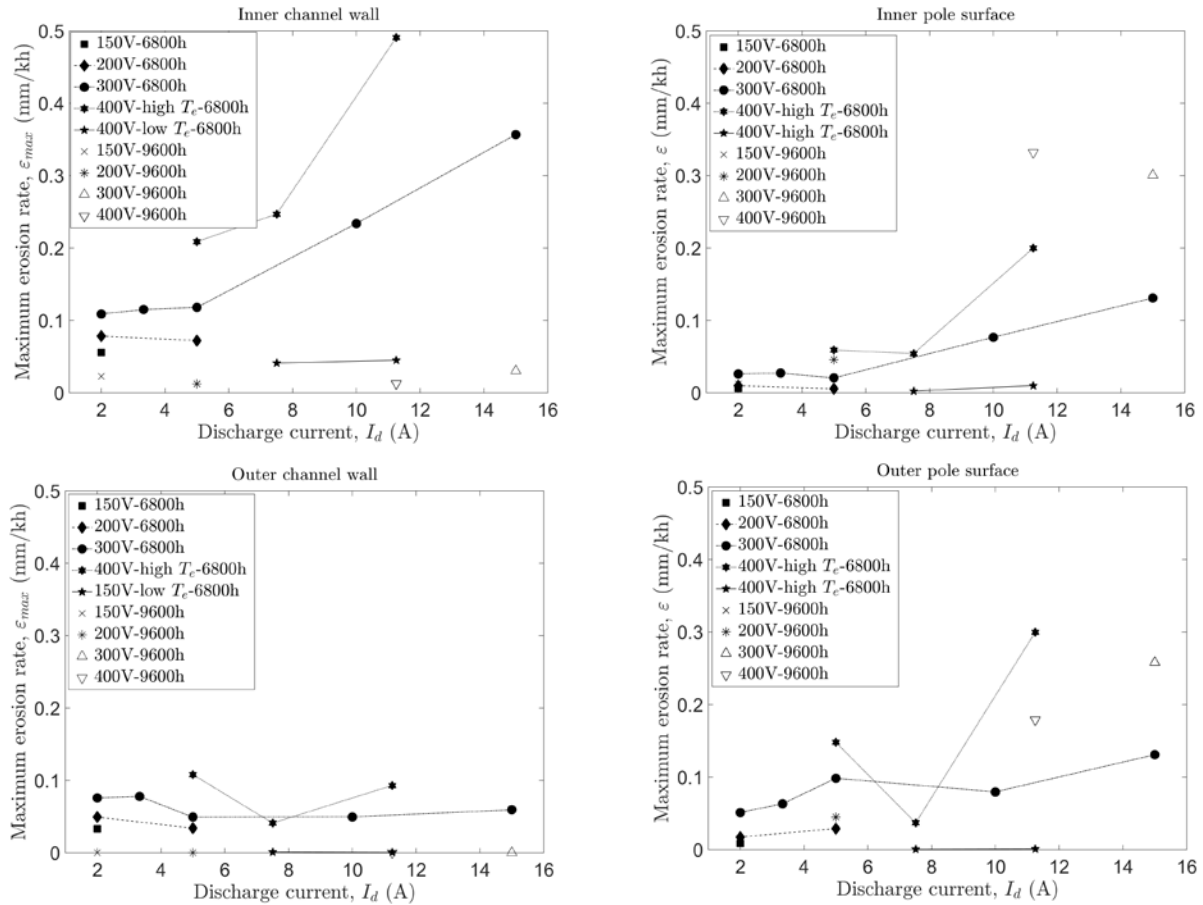


Fig. 13. Maximum erosion rates along the channel and pole walls as a function of the operating condition. Included in this chart are the maximum erosion rates for the tested high and low peak electron temperature profiles and a case at each discharge voltage run in the 9,600-h channel geometry.

described in Subsections V-a and V-b. The presentation used for the 400 V cases have been modified, linking by a dotted line the cases run with “high temperature profiles” that yield higher erosion rates (upper bound of erosion estimates) and with a continuous line the cases run with “low temperature profiles” (lower bound of erosion estimates). The erosion rates at 150, 200, and 300 V were computed using only “high temperature profiles” as indicated by the electron temperatures previously reported in Fig. 3. It can be observed that the erosion rates computed for the 400V-3kW (7.5A) case with the “high temperature profile” are consistent with the trends (i.e., erosion rates increasing with discharge current) observed for the 300 V cases and the 400V-2kW (5A) and 400V-4.5kW (11.25A) for the inner channel wall and inner pole cover. At the outer channel and pole, the erosion rate still decreases in the 400V-3kW case with respect to the other 400V conditions. However, the trend for these surfaces, as discussed in Section IV, is for the erosion rate to exhibit a lower rate of increase with discharge current or even stay relatively flat. As can be observed in Fig. 9 with more detail, the peak erosion rates for the outer surfaces are more than an order of magnitude higher than with the “low temperature profile” and within a factor of 2 to 4 of the predictions for the other 400 V cases.

One case at each discharge voltage run in the 9,600-h channel geometry has also been included. At the inner channel wall, the peak erosion rates are considerably reduced (by approximately an order of magnitude) in all cases due to better magnetic shielding of the walls in the 9,600-h configuration with respect to the 6,800-h geometry. For the outer channel walls, erosion does not occur. With respect to pole erosion, results for the both geometries are comparable in all cases, indicating that contrarily to what occurs at the channel walls, the erosion of the poles does not improve with time of operation. Peak erosion rates at high-power conditions are close to 0.3 mm/kh. This last result is most likely an upper bound of the pole erosion since, as discussed in Section III, uncertainties in the angular yield at high incidence angles (i.e., as seen in Fig. 6 and 11, beam ions that cause pole erosion describe trajectories that are almost parallel to the pole surfaces) are prone to produce an over-estimation of the erosion rates. Further evidence that our numerical results likely represent an upper bound of the pole erosion can be found in a rough estimation of the pole erosion in the QLT, based on the total erosion of the pole coatings through the test. This simple measurement indicates that, in the region where more erosion is found, the pole surfaces recess at a rate of approximately 0.25 mm/kh, which is slightly lower than our maximum predicted value. Without taking into account the possible over-estimation of the numerical estimates for the pole erosion rates, the alumina coating will not be completely eroded after 16,000 hours of operation (or 700 kg propellant throughput) at the most demanding condition.

VI. Cathode life assessment

In order to complete our discussion on the operating life of the XR-5 thruster, it is necessary to produce estimates of the expected cathode life. We use the JPL in-house Orificed Cathode (OrCa2D) code for this purpose. OrCa2D solves an extensive system of governing equations for the partially ionized gas in the interior and exterior of hollow cathodes. Development of the code began almost a decade ago and since then it has been used to simulate a variety of hollow cathodes operating under a wide range of conditions [41-46]. Comparisons with several plasma measurements (e.g. [47,48]) has helped improve both our understanding of driving processes inside these devices as well as the fidelity of the code. Like Hall2De, OrCa2D produces a 2-D map of the plasma properties inside the hollow cathode and its plume that can in turn be used to infer life estimates for the emitter and erosion rates at the walls. In this investigation, we use two cathode operating conditions. The first one assumes a mass flow rate of 0.34 mg/s (3.5 sccm) and discharge current of 1.67 A, representative of a low-power throttling condition of the XR-5. The second condition is defined by a mass flow rate of 1.14 mg/s (11.7 sccm) with a discharge current of 15 A and reproduces the cathode operating condition at the 400V-4.5kW throttling condition. For each current condition, the keeper was operated under both floating and current collection conditions, and the corresponding keeper voltage was computed self-consistently by the code. When in current-collection mode, the current to the keeper was specified at 1 A.

The emitter life is largely driven by its temperature, as suggested by the empirical expression [49],

$$t_{emitter} = \left(\frac{d_{emitter}}{100} \right)^2 \exp \left(\frac{3.2777}{T_{emitter}} \cdot 10^4 - 15.488 \right), \quad (8)$$

where the emitter thickness, $d_{emitter}$, temperature, $T_{emitter}$, and expected life, $t_{emitter}$, are in μm , K and hours. In OrCa2D simulations, the emitter temperature profile is required as input. This is typically provided to the code from

direct measurements (e.g. [50]). No such measurements were available for the cathode conditions investigated here. Thus in these investigations we proceeded to bound the problem by performing simulations by varying the maximum emitter temperature at each operating condition. The profile of the temperature along the emitter was held the same for all operating conditions and was specified based on measurements and simulations of a similar cathode.

When an excessively large temperature is employed in the simulations, the discharge current becomes very large. On the other hand, if the emitter temperature is set to a sufficiently low value, the emitter cannot produce enough current to support the discharge. Under these considerations, we are able to produce estimates of the maximum emitter temperature that range from 1050 to 1200 C. According to Eq. (8) and as seen in Fig. 14, the estimated emitter life exceeds 50,000 hours.

Erosion estimates for the orifice plate (tungsten) and keeper (stainless steel) surfaces were also produced based on the numerical results at the low and high power operating conditions for the cathode. The maximum erosion rate of all the examined cases was computed at the end of the orifice plate for the 15 A condition with a 0 A keeper and had a value of 2.7×10^{-3} mm/kh. This represents a maximum erosion of the walls of approximately 0.15 mm after 50,000 hours of operation, which should not constitute a threat for extended operation of the XR-5 cathode. We emphasize “maximum” since it is known that as the orifice plate erodes the erosion rates decrease due largely to a reduction of the plasma potential and, in turn, of the ion energy at the walls [41]. As shown in Table III, the maximum erosion rates for the low-power condition are almost an order of magnitude lower than for the high power condition. If the current collected by the keeper is set to 1 A, the erosion rates decrease by several orders of magnitude.

Other threats to extended operation of the cathode, such as plume mode or enhanced erosion due to plasma oscillations, cannot be assessed directly by OrCa2D simulations. However, based on previous tests, plume mode is highly unlikely to occur at 15 A due largely to the high flow rates employed at this condition. For the 1.67 A-case, plume mode was observed in the laboratory in a similar hollow cathode only at lower mass flow rates than the 30.34 mg/s used in the simulations. Plasma oscillations may be present and would require a measurement to confirm or not their presence. However, to date, performance, plume, and long-duration testing performed at JPL and Aerojet [2,24] has revealed no indications that operation at this low-current conditions have been detrimental to cathode health.

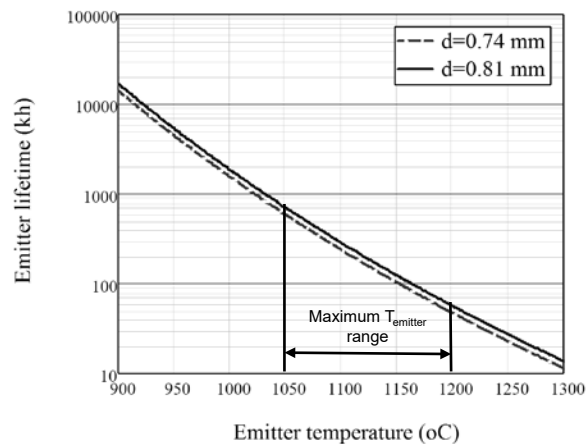


Fig. 14. Emitter lifetime as a function of emitter temperature (in degrees C). Life estimates in excess of 50,000 hours are predicted for the upper bound of the maximum emitter temperature.

| Cathode operating condition | | | | Maximum erosion rate (mm/kh) | |
|-----------------------------|-----------|-------------------|------------------|------------------------------|-----------------------|
| MFR (mg/s) | I_d (A) | $T_{emitter}$ (C) | I_{keeper} (A) | Orifice plate | Keeper surface |
| 0.34 | 1.67 | 1050 | 0 | 2.7×10^{-3} | 1.3×10^{-5} |
| 0.34 | 1.67 | 1050 | 1 | 1.1×10^{-6} | 1.9×10^{-12} |
| 1.14 | 15 | 1200 | 0 | 5.8×10^{-4} | 2.1×10^{-5} |
| 1.14 | 15 | 1200 | 1 | 3.6×10^{-9} | 0 |

Table III: Maximum erosion rates at the orifice plate and keeper surface for different cathode operating conditions

VII. Conclusion

We have assessed by numerical simulation the capability of the XR-5 thruster to be operated for periods of time in excess of 16,000 hours or with a total xenon throughput of 700 kg. Candidate phenomena for limiting thruster life are erosion of the channel walls and pole surfaces, and cathode emitter life an erosion of the cathode surfaces. The 2-D axisymmetric code Hall2De and the Orificed Cathode (OrCa2D) code were employed in these investigations. In a previous paper [23], distributions of anomalous collision frequencies were identified for eleven different throttling conditions of the XR-5 based on experimental measurements. In the first part of this paper, we computed maximum erosion rates at the thruster surfaces based on these profiles in a thruster channel geometry identical to that reached after 6,800 hours of operation during the Qualification Life Test of the XR-5. Results showed that the erosion of the channel walls was restricted to the downstream edges of the chamfered section (i.e., the rings) and $z/L > 0.95$ (with L being the length of the channel). The erosion rates were larger for the inner wall than for the outer wall and increased with discharge voltage due to ions being accelerated to higher velocities, and with discharge current due to the associated increased ion current density. Peak values of approximately 0.5 mm/kh were predicted for the more stringent operating condition of 400V-4.5kW. Erosion at the poles was found to peak at approximately 0.3 mm/kh. It was observed that erosion of the poles was mostly produced by beam ions due to the large divergence of the beam in the XR-5.

One result, at the 400V-3kW operating condition, was found not to follow the trends of the other conditions. At least one order of magnitude lower erosion rates were computed at this condition. A close investigation of the plasma properties along the channel centerline revealed a lower peak electron temperature value and higher values of the plasma potential in the plume region than those obtained in the simulations for other throttling conditions. These differences were found to be directly linked with the details of the anomalous collision frequency profile in this case, which was guided by electron temperature measurements that were possibly perturbed inside the acceleration channel. We showed that small modifications of the profile (particularly a shift downstream) produced erosion rate estimates that followed the trends marked by the other throttling conditions while the plasma properties and predicted performance remained within the uncertainties of the numerical measurements. As the two anomalous collision profiles used in these investigations produced reasonable results, we also performed sensitivity simulations with an anomalous collision frequency profile that yielded a low peak electron temperature in the 400V-4.5kW case. In a manner consistent with the results observed in the 400V-3kW case, this new profile resulted in lower erosion rates. We thus determined that the “low temperature” and “high temperature” profiles constituted a lower and upper bound, respectively, to the erosion rates.

As the maximum erosion rates predicted for the upper bound (or worst case scenario) were in the order of 0.5 mm/kh (albeit restricted to a very small region), we conducted additional simulations using the thruster geometry after 9,600 hours of Qualification Life Test. The erosion rates found in this configuration indicate that the erosion of the channel walls decreases as the geometry is progressively modified by the ion sputtering, eventually achieving a zero-erosion state. No significant differences were observed between the 6,800-h and 9,600-h configurations for the worst case scenario of erosion at the pole covers. Attending to the peak erosion rates predicted at the poles, the alumina coatings that protect the magnetic poles will not be eroded after 16,000 hours of operating at the most demanding high-power condition.

An assessment of the cathode expected life was conducted at two operating conditions representative to low and high power operation of the thruster. Results of these investigations suggest that the emitter life (estimated to be more than 50,000 hours) does not pose a threat to the operation of the thruster. Erosion of the orifice plate and keeper surfaces was found to be minimal. Phenomena such as plasma oscillations and plume mode are not captured

in OrCa2D and can potentially increase the erosion rates at the cathode surfaces. However, testing performed at JPL and Aerojet has revealed no indications of detrimental cathode health with time.

The combination of the results obtained for erosion of the thruster surfaces and cathode life show that the XR-5 Hall thruster will exceed 16,000 hours of operating life, which correspond to a propellant throughput in excess of 700 kg. These figures provide 50% margin over the usable throughput capability of 466 kg as already demonstrated in wear testing

Acknowledgments

The research described in this paper was carried out by the Jet Propulsion Laboratory, California Institute of Technology, under a contract with the National Aeronautics and Space Administration and funded through a Strategic Research and Technology Development program in JPL's Solar System Exploration Directorate. The experimental data on which the plasma simulations described here depend would not have been possible without the generous loan of the EM1 XR-5 that was provided by Aerojet Rocketdyne and Lockheed Martin. We would like to thank Vadim Khayms at Lockheed Martin for supporting the hardware loan and Alex Mathers at Aerojet Rocketdyne for preparing the thruster and providing support for the experiments throughout.

References

- [1] R. R. Hofer, T. M. Randolph, D. Y. Oh, J. S. Snyder, and K. De Grys, "Evaluation of a 4.5 kW commercial Hall thruster system for NASA science missions", AIAA paper 2006-4469, in proceedings of the 42nd AIAA/ASME/SAE/ASEE Joint Propulsion Conference, Sacramento, CA, 2006.
- [2] R. R. Hofer, D. M. Goebel, J. S. Snyder, and I. Sandler, "BPT-4000 Hall thruster extended power throttling range characterization for NASA science missions", IEPC-2009-085, in proceedings of the 31st International Electric Propulsion Conference, Ann Arbor, MI, 2009.
- [3] R. R. Hofer, "High-specific impulse operation of the BPT-4000 Hall thruster for NASA science missions", AIAA paper 2010-6623, in proceedings of the 46th AIAA/ASME/SAE/ASEE Joint Propulsion Conference, Nashville, TN, 2010.
- [4] K. De Grys, A. Mathers, B. Welander, "Demonstration of 10,400 hours of operation on a 4.5kW qualification model Hall thruster", AIAA paper 2010-6698, in proceedings of the 46th AIAA/ASME/SAE/ASEE Joint Propulsion Conference, Nashville, TN, 2010.
- [5] I. G. Mikellides, I. Katz, R. R. Hofer, D. M. Goebel, K. De Grys, and A. Mathers, "Magnetic shielding of the channel walls in a Hall plasma accelerator", *Physics of Plasmas*, Vol. 18, No. 3, 2011, pp. 033501.
- [6] W. A. Hoskins, R. J. Cassidy, O. Morgan, R. M. Myers, F. Wilson, and D. Q. King, "30 years of electric propulsion flight experience at Aerojet Rocketdyne", IEPC-2013-439, in proceedings of the 33rd International Electric Propulsion Conference, Washington, D.C., 2013.
- [7] L. Garrigues, G. J. M. Hagelaar, C. Boniface, and J. P. Boeuf, "Anomalous conductivity and secondary electron emission in Hall effect thrusters", *Journal of Applied Physics*, Vol. 100, No. 12, 2006, 123301.
- [8] J. C. Adam, A. Heron, and G. Laval, "Study of stationary plasma thrusters using two-dimensional fully kinetic simulations," *Physics of Plasmas*, Vol. 11, No. 1, 2004, 295.
- [9] A. Ducrocq, J. C. Adam, A. Heron, and G. Laval, "High-frequency electron drift instability in the cross-field configuration of Hall thrusters," *Physics of Plasmas*, Vol. 13, No. 10, 2006, 102111.
- [10] S. Tsikata, N. Lemoine, V. Pisarev, and D. M. Gresillon, "Dispersion relation of electron density fluctuations in a Hall thruster plasma, observed by collective light scattering," *Physics of Plasmas*, Vol. 16, No. 3, 2009, 033506.
- [11] J. Cavalier, N. Lemoine, G. Bonhomme, S. Tsikata, C. Honore, and D. Gresillon, "Hall thruster plasma fluctuations identified as the ExB electron drift instability: Modeling and fitting on experimental data", *Physics of Plasmas*, Vol. 20, 2013, 082107.
- [12] P. Coche and L. Garrigues, "A two-dimensional (azimuthal-axial) particle-in-cell model of a Hall thruster", *Physics of Plasmas*, Vol. 21, 2014, 023503.
- [13] I. Katz, I. G. Mikellides, B. A. Jorns and A. Lopez Ortega, "Hall2De simulations with an anomalous transport model based on the electron cyclotron drift instability", IEPC paper 2015-402, in Proceedings of the 34th International Electric Propulsion Conference, Kobe, Japan, 2015.
- [14] J. M. Fife, Ph.D. thesis, Massachusetts Institute of Technology, 1998.
- [15] P. Boeuf and L. Garrigues, "Low Frequency Oscillations in a Stationary Plasma Thruster," *Journal of Applied Physics*, Vol. 84, 1998, p. 3541.
- [16] G. J. M. Hagelaar, J. Bareilles, L. Garrigues, and J. P. Boeuf, "Two-dimensional model of a stationary plasma thruster", *Journal of Applied Physics*, Vol. 91, No. 9, 2002, pp. 5592-5598
- [17] F. I. Parra, E. Ahedo, J. M. Fife, and M. Martinez Sanchez, "A two-dimensional hybrid model of the Hall thruster discharge", *Journal of Applied Physics*, Vol. 100, No. 2, 2006.

- [18] I. G. Mikellides, I. Katz, and R. R. Hofer, "Design of a laboratory Hall thruster with magnetically shielded channel walls, phase I: numerical simulations", AIAA paper 2011-5809, in proceedings of the 47th AIAA Joint Propulsion Conference, San Diego, California, 2011.
- [19] B. A. Jorns, D. M. Goebel, and R. R. Hofer, "Plasma Perturbations in High-Speed Probing of Hall Thruster Discharge Chambers: Quantification and Mitigation", AIAA paper 2015-xxxx, in proceedings of the 51st AIAA/ASME/SAE/ASEE Joint Propulsion Conference, Orlando, Florida, 2015.
- [20] I. G. Mikellides and I. Katz, "Numerical simulations of Hall-effect plasma accelerators on a magnetic-field-aligned mesh", *Physical Review E*, Vol. 86, 2012, p. 046703.
- [21] A. Lopez Ortega and I. G. Mikellides, "A new cell-centered implicit numerical scheme for ions in the 2-D axisymmetric code Hall2De", AIAA paper 2014-3621, in proceedings of the 50th AIAA Joint Propulsion Conference, Cleveland, OH, 2014.
- [22] A. Lopez Ortega and I. G. Mikellides, "The importance of the cathode plume and its interactions with the ion beam in numerical simulations of Hall thrusters", IEPC-2015-310, in proceedings of the 34th International Electric Propulsion Conference, Kobe, Japan, 2015.
- [23] B. A. Jorns, R. R. Hofer, and I. G. Mikellides, "Power dependence of the electron anomalous collision frequency in a Hall thruster", AIAA paper 2014-3620, in proceedings of the 50th AIAA Joint Propulsion Conference, Cleveland, OH, 2014.
- [24] K. De Grys, B. Welander, J. Dimicco, S. Wenzel, and B. Kay, "4.5 kW Hall thruster system qualification status", AIAA paper 2005-3682, in proceedings of the 41st AIAA/ASME/SAE/ASEE Joint Propulsion Conference, Tucson, AZ, 2005.
- [25] B. A. Welander, and K. H. De Grys, "Completion of the BPT-4000 Hall thruster qualification, 53rd JANNAF Propulsion Meeting, Monterey CA, 2005.
- [26] K. De Grys, C. Carpenter, B. Welander, A. Mathers, and R. R. Hofer, "Extended duration operation of BPT-4000 qualification unit at low power", in proceedings of 3rd JANNAF Spacecraft Propulsion Joint Subcommittee Meeting, Orlando, FL, 2008.
- [27] R. R. Hofer, D. M. Goebel, J. S. Snyder, and I. Sandler, "BPT-4000 Hall Thruster Extended Power Throttling Range Characterization for NASA Science Missions," IEPC-2009-085, in proceedings of the 31st International Electric Propulsion Conference, Ann Arbor, Michigan, 2009.
- [28] R. R. Hofer, D. M. Goebel, B. A. Jorns, C. Garner, J. S. Snyder, I. G. Mikellides, M. Sekerak, and A. Mathers, "Long-life, high-Isp Hall thruster technology for primitive bodies", Annual report, Jet Propulsion Laboratory, California Institute of Technology, 2014.
- [29] I. Katz and I. G. Mikellides, "Neutral gas free molecular flow algorithm including ionization and walls for use in plasma simulations", *Journal of Computational Physics*, Vol. 230, 2011, pp. 1454-1464
- [30] G. D. Hobbs, and J. A. Wesson, "Heat Flow through a Langmuir Sheath in Presence of Electron Emission," *Plasma Physics*, vol. 9, no. 1, pp. 85-87, 1967.
- [31] Y. Garnier, V. Viel, J. F. Roussel, and J. Bernard, "Low-energy xenon ion sputtering of ceramics investigated for stationary plasma thrusters", *Journal of Vacuum Science and Technology A*, Vol. 17, 1999, pp. 3246-3254
- [32] Y. Yamamura and S. Shindo, "An empirical formula for angular dependence of sputtering yields", *Radiation Effects*, Vol. 80, 1984, pp. 52-72.
- [33] J. Bohdansky, J. Roth, and H. L. Bay, "An analytical formula and important parameters for low-energy ion sputtering", *Journal of Applied Physics*, Vol. 51, 1980, p. 2861.
- [34] A. P. Yalin, B. Rubin, S. R. Dominguez, Z. Glueckert, and J. D. Williams, "Differential sputter yields of boron nitride, quartz and kapton due to low energy Xe⁺ bombardment", AIAA paper 2007-5314, in proceedings of the 43rd AIAA Joint Propulsion Conference, Cincinnati, Ohio, 2007
- [35] W. Eckstein and R. Preuss, "New fit formulae for the sputtering yield", *Journal of Nuclear Materials*, Vol. 320, 2003, 209-213
- [36] *Sputtering by Particle Bombardment I*, R. Behrisch and W. Eckstein, eds. Springer, Berlin, 2007
- [37] M. Tartz, T. Heyn, C. Bundesmann and H. Neumann, "Measuring sputter yields of ceramic materials", IEPC paper 2009-240, in proceedings of 31st International Electric Propulsion Conference, Ann Arbor, Michigan, 2009
- [38] Y. Raitses, A. Smirnov, D. Staack, and N. J. Fisch, "Measurements of secondary electron emission effects in the Hall thruster discharge", *Physics of Plasmas*, Vol. 13, 2006, 014502
- [39] Kathe Dannemayer, "Scaling laws and electron properties in Hall effect thrusters", Universite d'Orleans, 2012.
- [40] A. Lopez Ortega, I. G. Mikellides and I. Katz, "Hall2De numerical simulations for the assessment of pole erosion in a magnetically shielded Hall thruster", IEPC-2015-249, in proceedings of the 34th International Electric Propulsion Conference, Kobe, Japan, 2015.
- [41] I. G. Mikellides, and I. Katz, "Wear mechanisms in electron sources for ion propulsion, 1: Neutralizer hollow cathode", *Journal of Propulsion and Power*, Vol. 24, No. 4, 2008, 855-865.
- [42] I. G. Mikellides, I. Katz, D. M. Gobel, K. K. Jameson, and J. E. Polk, "Wear mechanisms in electron sources for ion propulsion, 2: Discharge hollow cathode", *Journal of Propulsion and Power*, Vol. 24, No. 4, 2008, 866-879.

- [43] I. G. Mikellides, I. Katz, D. M. Goebel, and J. E. Polk, "Hollow cathode theory and experiment, II: A two-dimensional theoretical model of the emitter region", *Journal of Applied Physics*, Vol. 98, No. 11, 2005.
- [44] I. G. Mikellides, I. Katz, D. M. Goebel, J. E. Polk, and K. K. Jameson, "Plasma processes inside dispenser hollow cathodes", *Physics of Plasmas*, Vol. 13, No. 6, 2006.
- [45] I. G. Mikellides, D. M. Goebel, J. S. Snyder, I. Katz, and D. A. Herman, "The discharge plasma in ion engine neutralizers: Numerical simulations and comparisons with laboratory data", *Journal of Applied Physics*, Vol. 108, No. 11, 2010.
- [46] I. G. Mikellides, "Effects of viscosity in a partially ionized channel flow with thermionic emission", *Physics of Plasmas*, Vol. 16, No. 1, 2009.
- [47] D. M. Goebel, K. K. Jameson, R. M. Watkins, I. Katz and I. G. Mikellides, "Hollow cathode theory and experiment, I: Plasma characterization using fast miniature scanning probes", *Journal of Applied Physics*, Vol. 98, No. 11, 2005.
- [48] D. M. Goebel, K. K. Jameson, I. Katz, and I. G. Mikellides, "Potential fluctuations and energetic ion production in hollow cathode discharges", *Physics of Plasmas*, Vol. 14, No. 10, 2007.
- [49] D. Goebel and I. Katz, "Fundamentals of Electric Propulsion: Ion and Hall Thrusters", Wiley, 2008, p. 300.
- [50] J. E. Polk, C. M. Marrese-Reading, B. Thornber, L. Dang, L. K. Johnson, and I. Katz, "Scanning optical pyrometer for measuring temperatures in hollow cathodes", *Review of Scientific Instruments*, Vol. 78, No. 9, 2007.